NASA-CR-196939

[illegible]

[illegible]

26387

Final Technical Report

August 15, 1991 - August 14, 1994

UV Extinction and IR Emission in Diffuse HII Regions

Grant No: NAG5-1743

Principal Investigator:
Dr. Per A. Aannestad
Arizona State University
Tempe, AZ 85287

(NASA-CR-196939) UV EXTINCTION AND IR EMISSION IN DIFFUSE H2 REGIONS Final Technical Report, 15 Aug. 1991 - 14 Aug. 1994 (Arizona State Univ.) 33 p

N95-12244

Unclas

G3/46 0026389

I. Introduction

HII regions occupy a unique position in our understanding of the physical relationships between stars, the interstellar medium, and galactic structure. Understanding these relations is complicated as observations show a complex interaction between a newly formed hot star and its surroundings. In particular, the ultraviolet radiaton from the stars modifies the pre-existing dust, which again affects both the amount of ionizing radiation absorbed by the gas, and the infrared spectrum emitted by the heated dust. The aim of this project was to use UV and far-UV observations to gain information on the nebular dust, and to use this dust to model the far-IR emission, for a consistent picture of a few selected diffuse HII regions.

Using archival data from the IUE and Voyager data banks and computed model atmospheres (Kurucz 1992), we have deduced extinction curves for the early-type stars ζ Oph, ξ Per, and σ Sco. Obtaining suitable model spectra at the requisite spectral resolution turned out to be a major task (see §III below). We have successfully modelled (§IV below) these curves in terms of a multi-component, multi-size distribution of dust grains, and interpret the differences in the curves as primarily due to the presence or non-presence of intermediate size grains (0.01 - 0.04 μm). Much smaller (0.005 μm) grains must also be present. Finally, we have made calculations of the temperature fluctuations and the corresponding infra-red emission in such small grains (§V below). However, we have not yet finished the work of constructing overall far-infrared models to be compared with the IRAS data. Below we detail the results achieved during the time of this project.

II. Observational data

The stars ζ Oph, ξ Per, and σ Sco span much of the observed variation in the UV extinction for moderately reddened stars (E(B-V) $\approx$ 0.3 - 0.4). In addition, we used the star μCol as a standard in the usual "pair" comparison method for ζOph, in order to have a check on the present method of using model atmosphere standards. The IUE and Voyager data for these stars are listed in Table 1. In the case of ξ Per and σ Sco, no low-resolution spectra were present in the IUE data bank, and we instead used available high-resolution images, and averaged these by weights into bins of width 3 Å . Finally, due to poor wavelength calibration, we have shifted these spectra by an amount necessary to move the center of the Lyα absorption feature to 1215.7 Å . This shift is listed in the last column of Table 1. The spectra have also been corrected for atomic and molecular hydrogen absorption along the line of sight, following the procedures of Fitzpatrick and Massa (1990), and Snow, Allen, & Polidan (1990), respectively.

III. Model Standards

The usual "pair" method relies on finding an unreddened or slightly reddened comparison star of the same spectral class as the observed star. However, it is often difficult to find an exact spectral match, and a mismatch of even one spectral subclass can lead to large errors in the ultraviolet extinction. Also, any de-reddening of the comparison standard according to some "average" extinction curve provides an additional source of error. In this project, we have instead employed theoretical energy distributions for comparison. The principal uncertainty in this method is the (probable) lack of enough ultraviolet opacity in the model calculations, leading to an overestimate of the extinction. However, in the recent models of Kurucz (1992) a large number of additional line opacities as well as additional continuum opacities have been included, and extensive model grids in T_{eff} and log g are provided at a resolution of 10 Å . While there still may be deficiencies in the ultraviolet opacities, and there are uncertainties in the model input parameters such as T_{eff}, log g, abundances, and microturbulent velocities, using the intrinsically reddening-free model standards should give no more uncertain far-UV extinction than the traditional method. As a check on the relative agreement between the two procedures, we also derive the extinction curve for ζ Oph by comparing with its usual standard μ Col.

A fundamental difficulty in deriving an ultraviolet extinction curve is classifying the UV spectrum correctly in order to find the correct un-reddened UV standard. Fanelli et al. (1987) have defined a set of twelve far-UV spectral line indices based on IUE low-resolution spectra that may serve as temperature, luminosity and abundance discriminants, since line indices are quite unaffected by the unknown continuum extinction. The most direct way of picking a comparison model on this basis would be to compare the observed line indices with calculated theoretical indices as functions of T_{eff}, log g, abundance, and other input parameters. However, limitations in the current Kurucz models for hot stars such as the lack of NLTE, no inclusion of wind effects, and some opacity still missing, make calculated line indices quite uncertain. Comparing the observed indices with the empirical list of indices versus spectral class given by Fanelli et al. (1992) and then converting to temperature and gravity via the usual calibrations, is a less direct, but maybe "safer" way of obtaining a good comparison. Nevertheless, since not all theoretical line indices are equally subject to the mentioned limitations, we have used the models to calculate four selected indices as additional guides in choosing the model standard. Also, such calculations provide an estimate of how close the present Kurucz LTE models approximate some of the far-UV line absorptions.

The wavelength resolution of the Kurucz (1992) models as published is 10 Å while the line indices are defined as integrals over bandpasses typically only 20 Å in width. It has therefore been necessary to re-compute the theoretical spectra at a much higher resolution. We obtained software from R. Kurucz (1993, personal communication), converted it to run under UNIX and computed synthetic spectra at a resolution $\Delta\lambda/\lambda = 50{,}000$ for the wavelenght intervals of four selected indices. We have assumed solar abundances for the models, and the microturbulent velocity has been set to 2 km/s. The spectra have been rotationally broadened with a rotational velocity of 25 km/s, and smeared with a Gausssian profile corresponding to the IUE low-resolution instrumental profile of FWHM = 6.1 Å . The UV line index is defined as -2.5 $\log_{10} F_\lambda/F^c_\lambda$ where F_λ is the average flux density for the band in question and F^c_λ is the linearly interpolated flux density at the center of the band computed from the average flux densities in two bracketing sidebands (Fanelli et al. 1992).

In Figure 1 we show the four theoretical indices as functions of T_{eff} and $\log g$, as well as the observed line indices for seven main sequence stars (point stars) and five giant stars (luminosity class III) (point circles) as tabulated by

Fanelli et al. (1992). In plotting the latter, we have assumed the spectral class - T_{eff} calibration given by Schmidt-Kaler (1982). The stars are of spectral class B2 or earlier, and should therefore have metal abundances similar to solar, as assumed in the model spectra calculated here. The error bars represent an estimate of the minimum uncertainty in the spectral index using a relative uncertainty in the IUE flux levels of 0.03 (Massa, Savage, & Fitzpatrick 1983). The limiting upper temperature for the models, given a value of log g, is set by the model becoming unstable due to radiative acceleration ("blow-up"). We see that the model calculations show the same trend with temperature as the observed indices and are within the observational uncertainties for the lower temperatures. However, at the higher temperatures there appears to be a systematic overestimate of the line flux relative to the continuum by about 10 percent (change of 0.1 in the index). This is most probably due to still missing model line opacity, but this should not seriously affect the derived extinction, which is more sensitive to model continuum opacity. Considering all the far-UV indices in Figure 1, it does not appear possible at the present time to use these indices to determine an effective temperature to better than a few thousand degrees. On the other hand, this is comparable to the uncertainty of about one MK spectral subclass estimated for the "pair" method.

In Table 2 we list the far-UV line indices as determined from the IUE spectra of Table 1. The Kurucz grid model standard selected on the basis of these values and the Fanelli et al. observed values in Figure 1 are listed in the last column of Table 2. For the O stars, the model value of $\log g$ is the grid value closest to the value for the particular star as determined from fundamental parameters as estimated by Howarth and Prinja (1989). For the

B stars, the value is chosen based on the calibration tables of Schmidt-Kaler (1982).

In Figure 2 we compare the Kurucz model of T_{eff} = 33,000K, $\log g = 4.0$ with the two observed spectra of μ Col as well as with the intrinsic flux distribution for O9.5 V stars as deduced from two-colour diagrams by Papaj, Wegner, & Krełowski (1990). The spectra are normalized to the flux density at 2740 Å and shifted relative to each other by one dex for visibility. The μ Col spectra have been dereddened by applying an average UV-extinction curve (Seaton 1979) for E(B-V) = 0.01. We see that the Kurucz model continuum agrees very well both with the observed spectra of μ Col and with the O9.5V intrinsic spectrum, even for wavelengths below 1700 Å . It appears that current modelling can reasonably account for the far-UV continuum, justifying our use of the models as reddening-free standards.

IV. UV Extinction Curves

Using theoretical model spectra as comparison spectra, we have calculated extinction curves E(λ) = E(λ- V)/E(B-V) for ζ Oph, ξ Per, and σ Sco. The input values used in deriving the extinction for each star is listed in Table 3, and the curves are shown in Figure 3. The "gaps" are due to spurious structure removed near the hydrogen lines, the CIV line, and, for ζ Oph and ξ Per, near the Si IV line. For ζ Oph , we also show the extinction curves (dashed curves in Fig. 3a) derived from the "pair" comparison method using the dereddened and hydrogen-corrected spectrum 1 of μ Col (Table 1) as the standard spectrum. In this case we took E(B-V) = B-V - $(B\text{-}V)_0$ = 0.32 (Diplas & Savage 1993). Except for a slightly flatter minimum beyond the 4.6 μm^{-1}

extinction hump, using a computed model standard gives good agreement with the traditional "pair" method for the whole range of wavelengths.

In modelling these extinction curves, we assumed a multi-component size distribution of dust grains. There is a set of "very small grains" (Rayleigh limit) of dimension 50 Å, and a distribution n(a) $\propto a^{-3.5}$ of larger, spherical grains with radii in the range a_{min} to a_{max}, where the smallest value of a_{min} is 0.0156 μm, and the largest value of a_{max} is 0.25 μm. The larger grains are made of separate populations of silicate and carbonaceous (graphite or amorphous) grains, and the silicate grains may have a mantle of constant thickness, made of either graphitic material, amorphous carbon, or "organic refractory" material. The optical constants of silicate and graphite were taken from Draine (1985) and Draine & Lee (1984), respectively. For amorphous carbon we chose the optical properties as either given by Hageman, Gudat, & Kunz (1974), by the AC1 or BE1 optical constants of Rouleau and Martin (1991), or by Edoh's (1983) constants as listed by Hanner (1987). The optical constants of the organic refractory material are from Table 3 of Jenniskens (1993). The very small grains were assumed to have the composition of either graphite, the amorphous carbon types given above, or diamond. The optical properties of diamond were from Papadopoulos & Anastassakis (1991). Extinction cross sections are calculated via Mie-type calculations for homogenous spheres and coated spheres (Bohren & Huffman 1983). For the small graphite particles we also calculated extinction due to disks or anisotropic ellipsoids, using the Discrete Dipole Approximation (Draine 1988). In addition, we include a component of Polycyclic Aromatic Hydrocarbons (PAHs), with absorption cross sections from Figure 1 of Joblin, Léger, &

Martin (1992) and from Puget & Léger (1989).

A given model thus has five possible ingredients, large and small silicate grains, large and small carbonaceous grains, and the PAH's. In addition, the large silicate grains may have mantles. After choosing the detailed material compositions, and the ranges for the size distributions of the larger grains, we have fitted the model extinction to the observed extinction curve by nonlinear χ^2- minimization, varying the fractional amount of cosmic Si and C that are locked up in each ingredient. Calculations covering a range of compositions, and different size ranges indicate through the χ^2- value what constitutes the "best" fit. If the ratio of visual to selective extinction (R_V) is known, we also required that the model gave a value close to observed value. It is important to note that since we fitted to *relative* extinction values, only the relative fractional amounts of Si and C get determined. Changing all the fractional depletions in the various ingredients by one and the same factor produces the identical $E(\lambda)$ and R_V. The values given in the figures are values that are closest to the absolute level of visual extinction. Also, the assumed cosmic abundances of C and Si ($C/H = 4.7\times10^{-4}$ [Lambert 1978], $Si/H = 3.5\times10^{-5}$) determine the relative and absolute levels of extinction. The solar carbon abundance may be lower by about 15 percent ($C/H = 4\times10^{-4}$, Grevesse et al. 1991), and the model fractional dust amounts should then be increased by a factor of 1.18. Finally, the material densities assumed are 3.3 gcm^{-3} for silicate, 2.3 gcm^{-3} for graphite, 1.5 gcm^{-3} for amorphous carbon, and 3.5 gcm^{-3} for diamond.

While we have searched in the somewhat arbitrarily limited parameter space of $[a_{min}, a_{max}] = [0.0156\mu m, 0.25\mu m]$ for the best fit solutions, there is no absolute guarantee that a set of very different values cannot give equally good or better fits. An extensive global optimization program over a much larger region and including simultaneously all the possible material ingredients would be valuable, but is outside the scope of this investigation. In some cases we have included seven simultanous ingredients (small and large silicates, small and large graphite, small and large amorphous carbon, and PAHs), but without significantly changed results.

For the random errors in the observational data we assume (Massa, Savage, & Fitzpatrick 1983)

$$\sigma[E(\lambda)] = \frac{\{\sigma_1^2 + 2.25 \times 10^{-4}[1 + E^2(\lambda)]\}^{1/2}}{E(B-V)}. \qquad (2)$$

For IUE observations $\sigma_1 \approx 0.03$, while for the Voyager data $\sigma_1 \approx 0.05$. For the Voyager part of the stellar spectrum we have the additional uncertainty due to the H_2 correction, and we estimate that in this range the total error is $\sigma_1 \approx 0.07$.

The systematic errors due to incorrect T_{eff} or log g can be investigated by calculating extinction curves based on different Kurucz model standards. However, for the hottest chosen standard (log g =4.0, T_{eff} =37,500K), no stable models exist for a higher temperature. We have therefore calculated relative extinction curves at the nearest model grid point where models for T_{eff}±2,000K and log g ± 0.5 do exist, assuming that approximately the same ratios apply at the higher temperatures. For each program star we calculate an "upper" and a "lower" extinction curve corresponding to variations in T_{eff} of ±2000K and in log g of ±0.25.

In Figure 4a we show the extinction curve for ζ Oph obtained from co-adding the two spectra (solid curves) in Figure 3a, using the Kurucz model

(Table 2) as the standard. The bars denote the random errors at each wavelength point as calculated from equation (2). The dashed line is the "best fit" model, and the solid curves represent the systematic "error envelope" (no random error included) as discussed above. Indicated in the Figure are the cosmic fractions of Si and C present in each grain population. Substituting any of the amorphous carbon grains for the graphite grains in this figure or adding a mantle of amorphous carbon to the silicates cannot give reasonable agreement with the observed curve, although a simultaneous presence of large and small amorphous carbon grains at the level of a few percent in the carbon fraction cannot be ruled out. An increase in the carbon PAH fraction from 0.03 to 0.075 with a simultaneous decrease in the graphite fractions (to 0.33 and 0.05) would give a slightly better fit, but the R_V value would be significantly too low (2.7) compared to the observed value of 3.09 (Cardelli, Clayton, & Mathis 1989). The main discrepancies between the model extinction and the observations in Figure 4a is a predicted slightly higher extinction peak at 4.6 μm^{-1} and a lower minimum at about 6 μ m^{-1}. The latter can be slightly improved by changing a_{min} from 0.0156 μm to 0.021 μm, as shown in Figure 4b, although the extinction peak then moves to about 4.7 μm^{-1} and the predicted R_V value decreases to 2.93. However, if we instead fit the the ζ Oph extinction curve using μ Col as the standard, the fits in this region are significantly improved, as shown in Figure 5. Figure 5a shows the coadded extinction (dashed curves in Fig. 3a) with the same model curve as in Figure 4a. The χ^2-value decreases by more than a factor of two. This may indicate that the Kurucz model standards used for ζ Oph are slightly deficient in continuum opacity in the particular wavelength interval of 1600 - 1800 Å as compared to real stars. Adding a small amount of amorphous carbon (BE1) as very small grains further improves the fit, but only slightly, as shown in Figure 5b.

In Figure 6 we show the best fit models for ξ Per, for which the observed R_V value is 3.40 (Cardelli et al. 1989). These fits differ from the ζ Oph case mainly in the lack of very small (0.005 μm) silicate grains and in no PAHs being present above a level of a few percent of the cosmic abundance of carbon. The graphite peak in Figure 6a is at slightly shorter wavelengths than in the observations, and an overall better fit is achieved by changing the 0.005 μm spherical graphite grains to oblate ellipsoids of axial ratio 2:1 and the same volume ($a_{VSG,equiv} = 0.005\mu$m), and increasing the minimum size for the larger graphite grains from 0.016 μm to 0.04 μm. This is shown if Figure 6b. As in the case of ζ Oph, but to a smaller degree, we note the increased extinction relative to the model in the region around 6 μm^{-1}, possibly indicating a slight deficiency in Kurucz model opacity for this region.

Figure 7 shows the results for σ Sco. The strong deviation in the lower envelope curve from the data points is mostly due to the sensitivity of the far-UV flux to a decrease in temperature of the model atmosphere from 25,000K to 23,000K. As shown in Figure 7a, the flat UV extinction can be very well fit by imposing a lack of both silicate and graphite grains with sizes in the range 0.01 - 0.04 μm, and no presence of PAHs above a few percent of the cosmic carbon abundance. However, the graphite peak is clearly at too short wavelenghts, and Figure 7b shows a much improved fit by again, as in the case of ξ Per, replacing the spherical very small graphite grains with 2:1 oblate ellipsoids. In both cases the predicted R_V values are close to the observed value of $R_V = 3.80$ (Cardelli et al. 1989).

V. Far-infrared emission.

The small grains required to explain the UV extinction are subject to temperature fluctuations when immersed in a diffuse radiation field. They therefore contribute to the emission over a large wavelength range, and, in particular, give emission at much shorter wavelengths than if they emitted at their equilibrium temperature. Figure 8 shows the emission of a graphite (solid curve) and a silicate grain (dotted curve) with radii of 0.005 μm, for a typical interstellar radiation field. The graphite grain emits more energy than the silicate grain at all wavelengths, but the emission falls off rapidly below about 30 μm. Since IRAS measured substantial flux densities at both 25 and 12 μm, additional dust emission is required. We have found that the 25 μ m emission may be increased substantially if the dielectric constant for small graphite grains has no contribution from conduction electrons. This follows from the semiconductor properties of graphite and graphite sizes $\leq$0.005 μm. The dashed curve in Figure 8 shows the emission from such a graphite grain, increasing the flux density at 25 μm by about an order of magnitude.

Figure 9 shows the far-infrared energy distribution for a size distribution of graphite and silicate grains in the range 0.0156 μm - 0.25 μm with the added contribution of the thermally fluctuating 0.005 μm grains. The solid curve assumes a normal dielectric function for the graphite grains, while the dashed curve assumes no conduction electrons present in the 0.005 μm graphite grains. The radiation field is a typical interstellar field, and the relative fractions of Si and C locked up in the grains are 0.9, 0.08. 0.45, and 0.1 for the large Si, small Si, large graphite, and small graphite grains, respectively. The 60 μm/100 μm flux density ratio of these curves is close to the values observed by IRAS for dust clouds.

VI. Conclusions

The main conclusions to be drawn from our modelling of ultraviolet diffuse extinction curves by size distributions of silicate and carbonaceous grain mixtures are:

1. Acceptable fits require that graphite is the main carbon component. The various amorphous carbon materials cannot substitute for the graphite grains, although such materials may be present at the level of a few percent of the cosmic carbon abundance. Also, amorphous carbon or "organic refractory" mantles on the silicate grains do not provide acceptable fits to the present extinction curves. On the other hand, small diamond grains (Rayleigh limit) may substitute for some or most of the small silicate grains.

2. Using optical properties of laboratory PAHs gives model fits that limit the carbon fraction in neutral PAHs to at most a few percent. Also, a substantial presence of PAHs would tend to lower R_V to unacceptable levels. However, ionized species of PAHs may have quite different optical properties, and, although not required in the present fits, may still be important contributors to the UV extinction curve.

3. The range in the ultraviolet extinction curves as represented by the curves of ζ Oph and σ Sco can be understood as mostly due to a variation in the presence of grain sizes $\sim$ 0.01 - 0.04 μm. The "flat" extinction curve of σ Sco demands a lower limit for the power law size distribution of $a_{min} \sim 0.04$ μm, but with still a substantial number of grains in the Rayleigh limit (here

0.005 μm). The intermediate extinction curve of ξ Per can be similarly well modelled if no silicate Rayleigh-size particles are present.

4. The best fits to the 4.6 μm^{-1} extinction hump in the curves of ξ Per and σ Sco is obtained if the Rayleigh-size graphite grains are 2:1 oblate disks.

5. For $R_V \geq 3.4$, the far-UV extinction may deviate significantly from the mean R_V-dependent extinction law of Cardelli et al. (1989).

6. Theoretical stellar atmosphere models (Kurucz 1992) may be used as reddening-free comparisons, even at far-UV wavelenghts, although some continuum opacity may still be missing in the region around 1700 Å. Theoretical UV line indices are systematically low compared to the observations, and cannot at the present time be used for accurate spectral classification.

7. Calculations of the spectrum of far-infrared radiation from a size distribution of silicate and graphite grains, including the contribution from thermally fluctuating 0.005 μm particles show agreement with IRAS observations of dust clouds for the 100 μm, 60 μm, and 25 μm wavelength bands. The 25 μm agreement requires that the small graphite grains have no conduction electrons due to their small size. The observed 12 μm emission, however, seems to demand the presence of molecular - size particles.

I am indebted to R. Kurucz for the use of his model atmospheres and spectral synthesis programs, to R. Polidan for the H_2 correction files, and to B. Draine for the use of the DDSCAT extinction program. I also want to thank P. Martin for sending data on amorphous carbon materials and C. Joblin for data on laboratory PAHs. Finally, I acknowledge useful dicussions with D. Burstein

and P. Hauschildt.

VII. Abstract: UV Extinction to 10.8 μm^{-1}

(Submitted to The Astrophysical Journal)

UV extinction curves that represent observed variations in diffuse clouds (ζ Oph, ξ Per, and σ Sco) have been derived by combining IUE and Voyager data and have been modelled by a multi-component size distribution of silicate and carbonaceous grains. We have used theoretical model atmospheres as our reddening-free standards, and, in the case of ζ Oph, also compare with the use of a stellar standard. An attempt was made to classify the UV spectra via theoretical spectral indices, but still missing line opacity appears to limit the use of this method at the present. The modelling includes five possible grain ingredients, large (0.015 - 0.25 μm) and small (0.005 μm) silicate grains, similarly large and small carbonaceous grains, and PAHs. The observed extinction curves are fitted by the model via nonlinear χ^2- minimization, varying the fractional amount of cosmic Si and C that are locked up in each ingredient. The observed variation from "steep" to "flat" UV extinction curves is found to correspond to a modest model variation in the lower limit of the power-law size distribution of the large grains. Graphite is found to be a necessary grain ingredient that cannot be replaced by the laboratory amorphous carbon materials. Carbonaceous mantles on the larger silicate grains provide no good fits to the observed curves. Using absorption properties of neutral laboratory PAHs limits PAHs to a few percent of the cosmic C abundance for acceptable fits that also give values for R_V close to the observed values.

TABLE 1. UV Data.

Star	HD #	IUE Images	Voyager # Year/Day	Spectrum # [a]	Shift (Å)
ξ Per	24912	SWP37373 LWR14987	Voy 1 81/083	1^b	0 Å
		SWP37376 LWR14988	Voy 2 80/178	2^b	0 Å
σ Sco	147165	SWP11064 LWP18630	Voy 1 80/177	1^b	0 Å
		SWP39508 LWP18631	Voy 1 80/177	2^b	0 Å
ζ Oph	149757	SWP32894 LWP12637	Voy 2 84/347	1	+2.0 Å
		SWP18252 LWR14381	Voy 2 84/347	2	+1.0 Å
μ Col[c]	38666	SWP25386 LWR17657	Voy 1 81/281	1	+1.5 Å
		SWP41195 LWP19996	Voy 1 81/281	2^b	0 Å

Notes to TABLE 1

[a] b: IUE high-resolution data of bin widths 3 Å .

[c] Comparison star for ζ Oph.

TABLE 2. Far-UV Stellar Indices and Model Standards

Star	Type	Spectrum	SiIV 1397	BL1425	FeV1453	BL1617	$T_{eff}, \log g^a$
ξ Per	O7.5 III	1	0.17	0.12	0.16	0.26	35,000 4.0
		2	0.14	0.13	0.16	0.25	
σ Sco	B1 III	1	0.34	0.10	0.05	0.11	25,000 3.5
		2	0.39	0.12	0.02	0.13	
ζ Oph	O9.0 V	1	0.18	0.16	0.11	0.17	35,000 4.0
		2	0.19	0.13	0.09	0.20	
μ Col	O9.5 V	1	0.19	0.11	0.04	0.19	33000, 4.0
		2	0.21	0.15	0.08	0.19	

Notes to TABLE 2

[a] Selected Kurucz grid model standard.

TABLE 3. Input Data and E(B-V)

Star	Log N(H)[a]	Log $N(H_2)$[b]	V[a]	B - V[a]	E(B-V)[a]	E(B-V)[c]
ξ Per	21.05	20.52	4.03	0.01	0.33	0.32
σ Sco	21.38	19.79	2.88	0.13	0.39	0.40
ζ Oph	20.69	20.64	2.56	0.02	0.32	0.33
μ Col	19.84	15.5	5.16	-0.29	0.01	...

Notes to TABLE 3

[a] Diplas & Savage (1993); [b] Bohlin *et al.* (1978); [c] Present model calculation

REFERENCES

Bohlin, R. C., Savage, B. D., & Drake, J. F. 1978, ApJ,224,132

Bohren, C. F., & Huffman, D. R. 1983, Absorption and Scattering of Light by Small Particles (New York: John Wiley & Sons)

Cardelli, J. A., Clayton, G. C., & Mathis, J. S. 1989, ApJ,345,245

Diplas, A., & Savage, B. D. 1993, preprint

Draine, B. T. 1985, ApJS,57,587

__________.1988, ApJ,333,848

Draine, B. T., & Lee, H. M. 1984, ApJ,285,89

Edoh, O. 1983, Ph. D. Thesis, University of Arizona

Fanelli, M. N., O'Connell, R. W., Burstein, D., & Wu, C.- C. 1992, ApJS,82,197

Fanelli, M. N., O'Connell, R. W., & Thuan, T. X. 1987, ApJ,321,768

Fitzpatrick, E. L., & Massa, D. 1990, ApJS,72,163

Grevesse, N., Lambert, D. L., Sauval, A. J., van Dishoeck, E. F., Farmer, C. B., & Norton, R. H. 1991, A& A,242,488

Hageman, H.- J., Gudat, W., & Kunz, C. 1974, DESY SR-47/7 (Hamburg:Deutsches Elektronen-Synchrotron)

Howarth, I. D., & Prinja, R. K. 1989, ApJS,69,527

Joblin, C., Léger, A., & Martin, P. 1992, ApJ,393,L79

Kurucz, R. L. 1992, in The Stellar Populations of Galaxies, eds. B. Burbay & A. Renzini (Kluwer, Dordrecht)

Massa,D., Savage, B. D.,& Fitzpatrick, E. L. 1983, ApJ,266,662

Papadopoulos, A. D., & Anastassakis, E. 1991, Phys.Rev.B,43,5090

Papaj, J., Wegner, W., & Krełowski, J. 1990, MNRAS,246,408

Puget, J. L., & Léger, A. 1989, ARA& A,27,161

Rouleau, F., & Martin, P. G. 1991, ApJ,377,526

Schmidt-Kaler, Th. 1982, in Numerical Data and Functional Relationships in Science and Technology Group VI,Vol. 2b,Section 4,453, ed. K. Schaifers & H.H.Voigt (Berlin:SpringerVerlag)

Snow, T. P., Allen, M. M., & Polidan, R. S. 1990, ApJ,359,L23

Figure Legends

Fig. 1. - Lines, theoretical line indices as functions of the effective stellar temperature computed from the models of Kurucz (1992). Valoes of $\log g$ as indicated. Circles and stars, observed line indices for main sequence stars and giants, respectively (from Fanelli et al. 1992).

Fig. 2. - Spectra normalized to the flux at 2740 Åwith arbitrary offsets of C. Curve for C = 0, the dereddened (E[B-V]=0.01) spectrum of μ Col using low-resolution IUE data and Voyager data. Curve for C = -1, the μ Col spectrum using binned high-resolution IUE data. Curve for C = +1, the spectrum from the Kurucz (1992) model with T_{eff} = 33,000K, log g = 4.0, and solar abundances. Curve for C = +2, the empirical intrinsic flux distribution for O9.5V stars (Papaj et al. 1990).

Fig. 3. - Normalized extinction curves derived from the spectra (1 and 2) of Table 1. Solid curves, using Kuruzc model standards as listed in Table 2. Curves (2) have been arbitrarily displaced upward by 3 units for clarity. Dashed curves, μ Col as standard (ζ Oph only). For clarity, dashed curves (1) and (2) have been displaced by -1 and +4 units, respectively.

Fig. 4. - Dashed curves, χ^2 - fits to coadded, normalized extinction data (Fig. 3a) for ζ Oph with a theoretical model standard. Bars show 1σ observational errors. Solid curves, observed extinction curves for a comparison model variation of ±2,000K in T_{eff} and ± 0.25 in log g. Dust model parameters as indicated. Si and C values refer to the fraction of cosmic abundances tied up in the larger grains and in the very small grains, respectively. R_V is the model value for the ratio of visual to selective extinction.

Fig. 5. - Solid curves, χ^2 - fits to coadded, normalized extinction data for ζ Oph with μ Col as standard star. Notation as in Fig. 4. Note the better fit at about 6 μm^{-1} compared to Fig. 4.

Fig. 6. - Dashed curves, χ^2 - fits to coadded, normalized extinction data (Fig. 3b) for ξ Per. Notation as in Fig. 4.

Fig. 7. - Dashed curves, χ^2 - fits to coadded, normalized extinction data (Fig. 3c) for σ Sco. Notation as in Fig. 4.

Fig. 8. - Solid curve, the emitted spectrum of a 0.005 μm graphite grain exposed to an average interstellar radiation field. Dotted curve, the spectrum for a silicate grain.

Fig. 9. - Solid curve, the infrared energy distribution for a size distribution of graphite and silicate grains in the range 0.0156 - 0.25 μm with the added contribution of thermally fluctuating 0.005 μm grains. Dashed curve, no contribution to the dielectric constant from conduction electrons for the 0.005 μm graphite grains. The grains are exposed to a typical interstellar radiation

field.

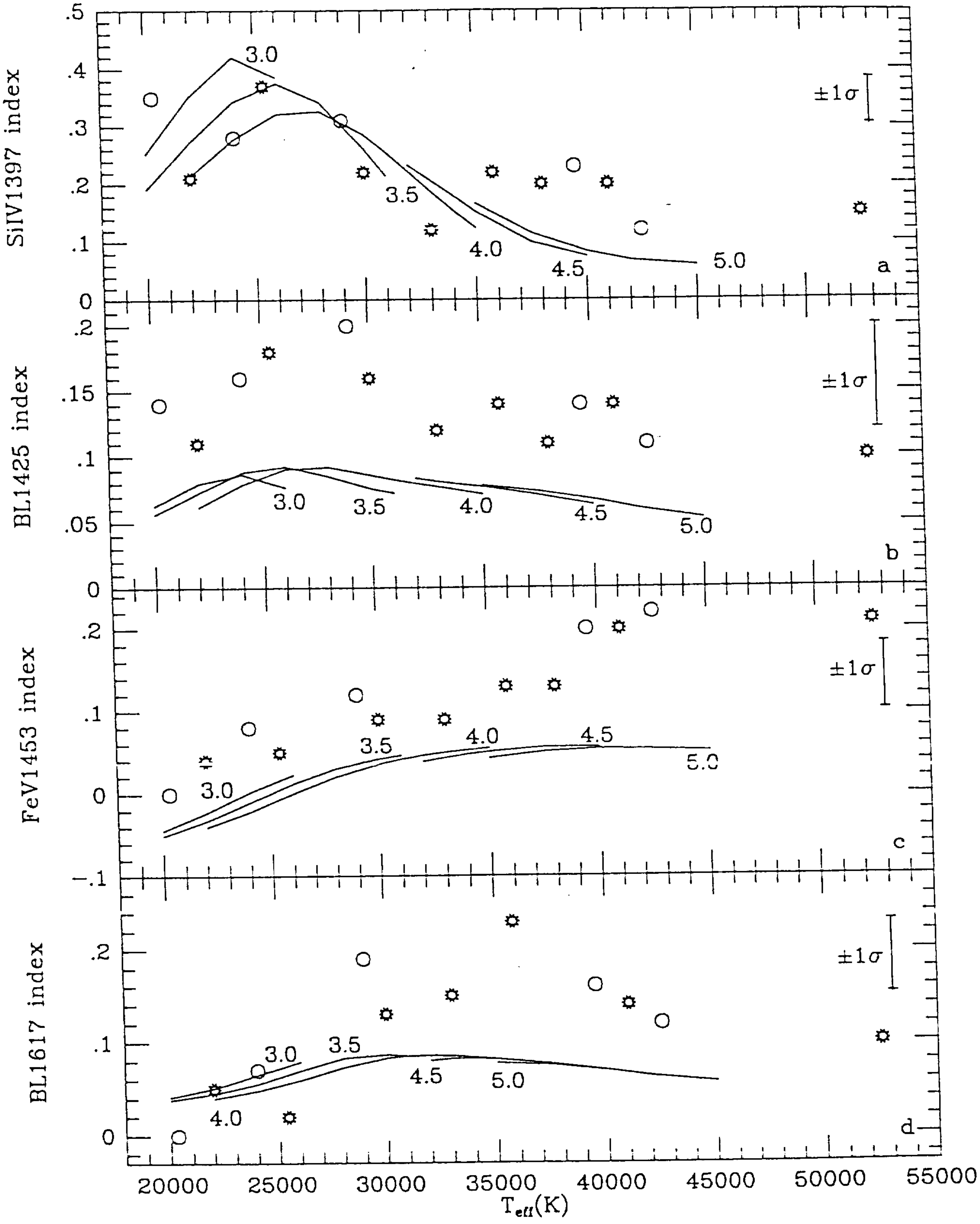
SiIV1397 index
BL1425 index
FeV1453 index
BL1617 index
.5
.4
.3
.2
.1
0
.2
.15
.1
.05
0
.2
.1
0
−.1
.2
.1
0
3.0
3.5
4.0
4.5
5.0
±1σ
a
b
c
d
20000
25000
30000
35000
40000
45000
50000
55000
T_{eff}(K)

Figure 1

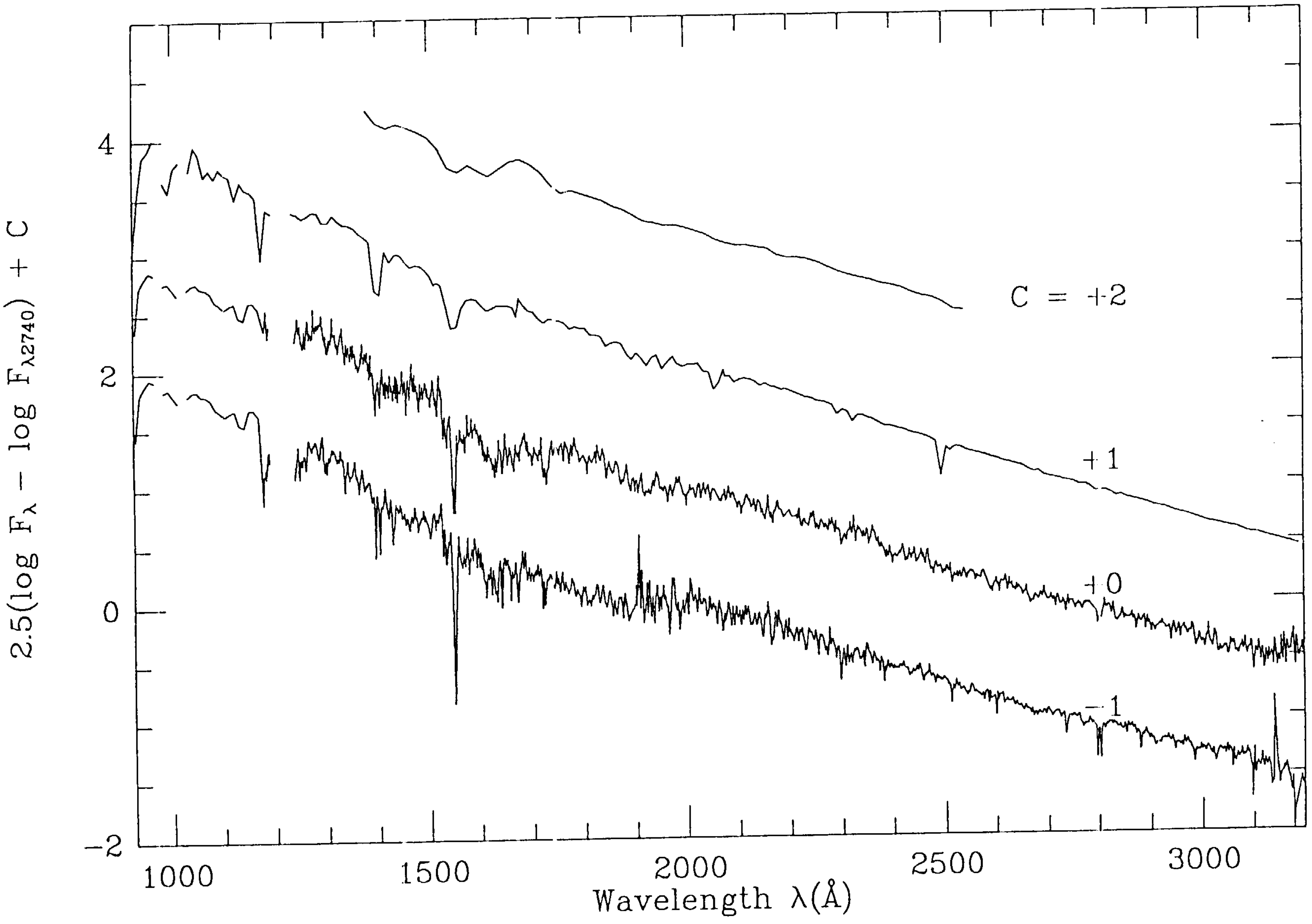
C = +2
+1
+0
−1
2.5(log F$_\lambda$ − log F$_{\lambda 2740}$) + C
4
2
0
−2
1000
1500
2000
2500
3000
Wavelength λ(Å)

Figure 2

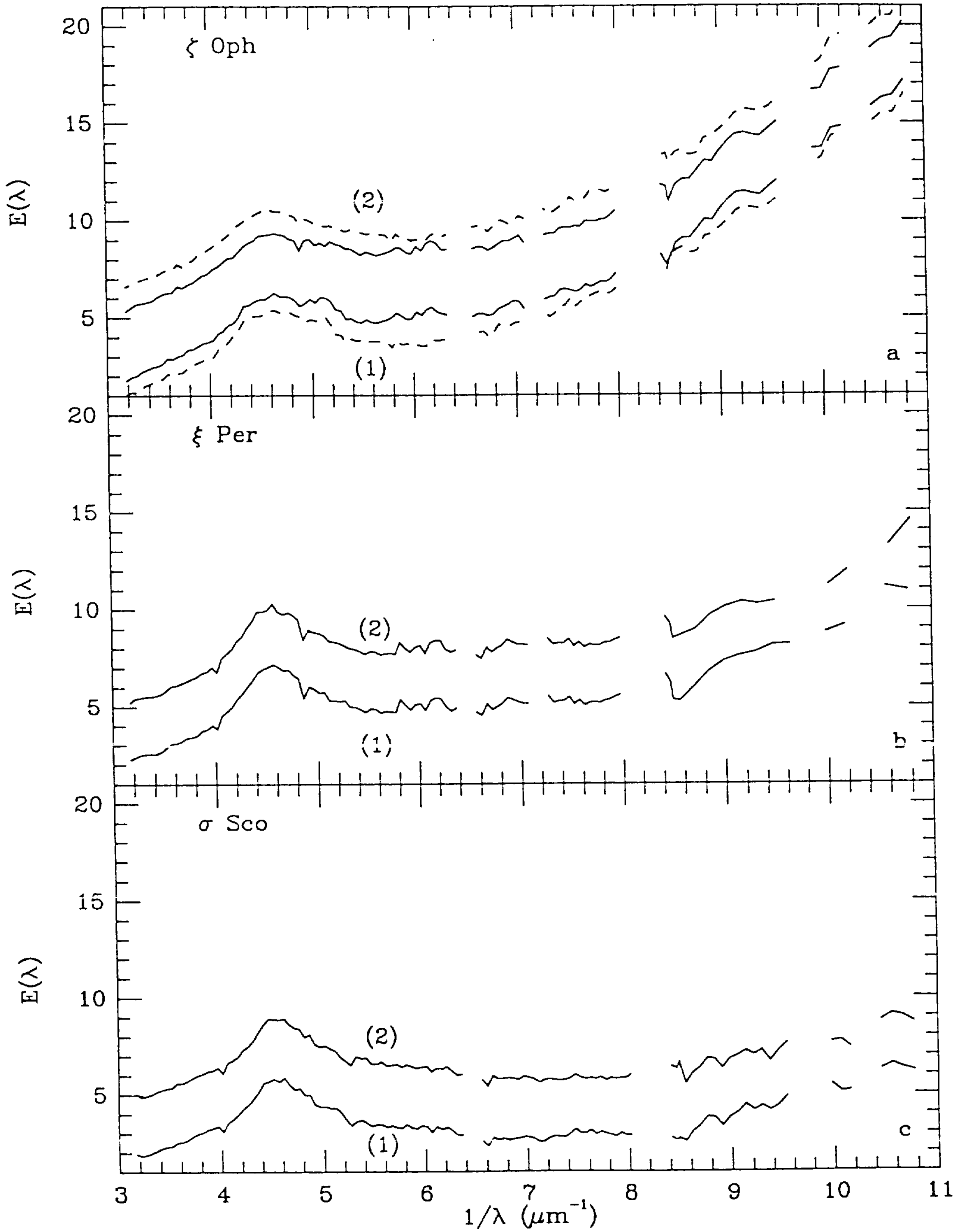

Figure 2

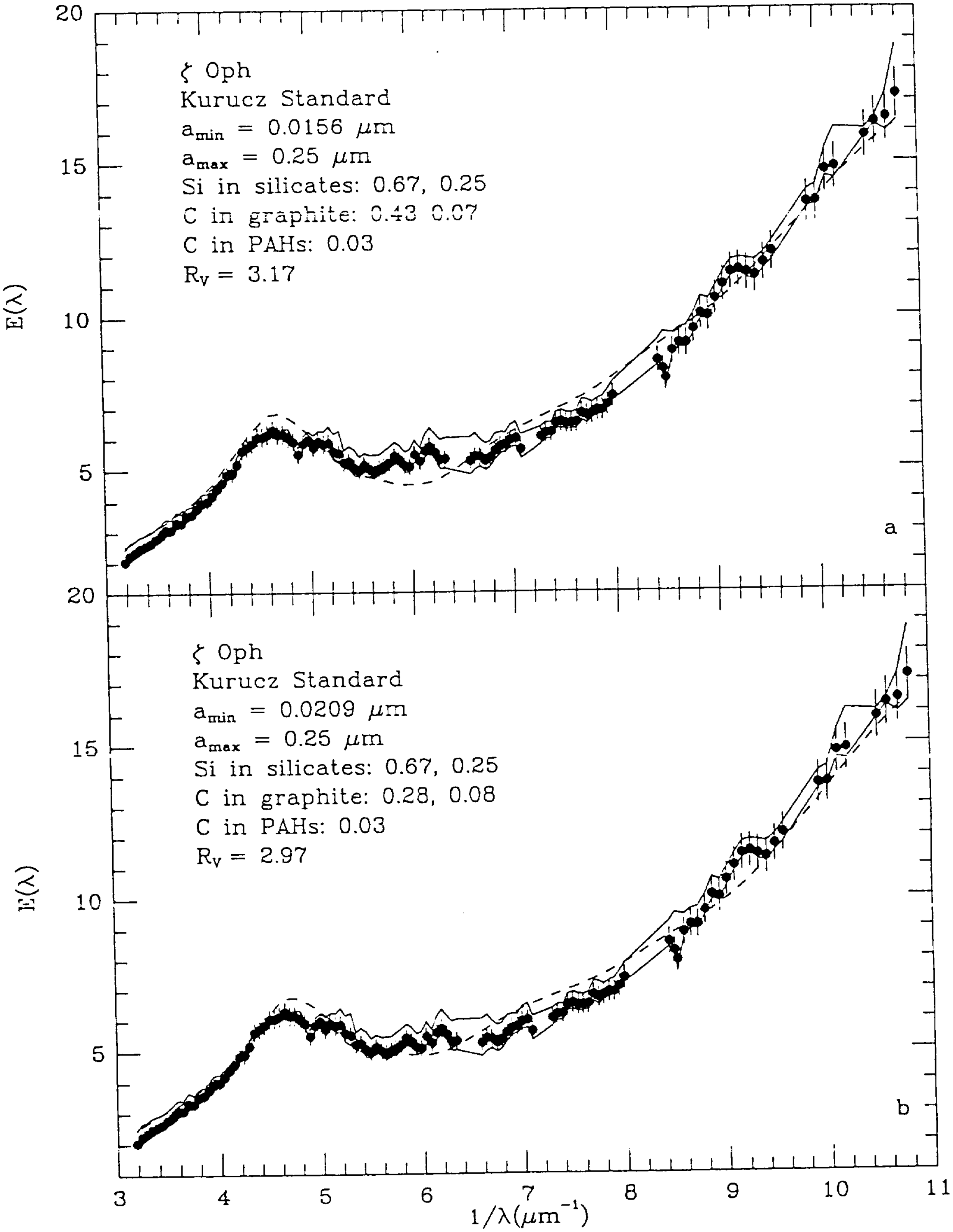

20
15
10
5
E(λ)
ζ Oph
Kurucz Standard
a_{min} = 0.0156 μm
a_{max} = 0.25 μm
Si in silicates: 0.67, 0.25
C in graphite: 0.43, 0.07
C in PAHs: 0.03
R_V = 3.17
a
20
15
10
5
E(λ)
ζ Oph
Kurucz Standard
a_{min} = 0.0209 μm
a_{max} = 0.25 μm
Si in silicates: 0.67, 0.25
C in graphite: 0.28, 0.08
C in PAHs: 0.03
R_V = 2.97
b
3
4
5
6
7
8
9
10
11
1/λ(μm^{-1})

Figure 4

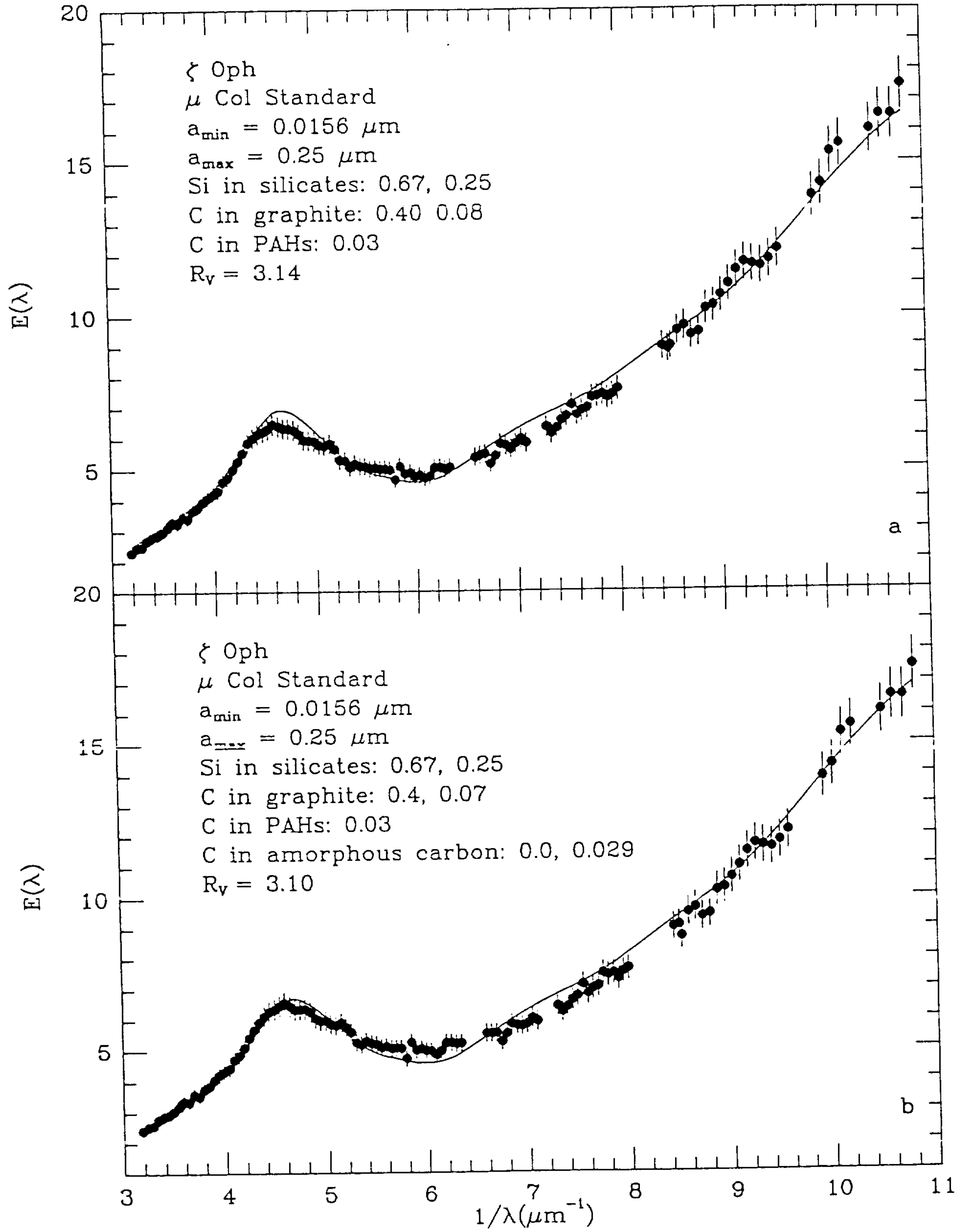
ζ Oph
μ Col Standard
a_{min} = 0.0156 μm
a_{max} = 0.25 μm
Si in silicates: 0.67, 0.25
C in graphite: 0.40 0.08
C in PAHs: 0.03
R_V = 3.14
a
ζ Oph
μ Col Standard
a_{min} = 0.0156 μm
a_{max} = 0.25 μm
Si in silicates: 0.67, 0.25
C in graphite: 0.4, 0.07
C in PAHs: 0.03
C in amorphous carbon: 0.0, 0.029
R_V = 3.10
b
E(λ)
E(λ)
20
15
10
5
20
15
10
5
3
4
5
6
7
8
9
10
11
1/λ(μm^{-1})

Figure 5

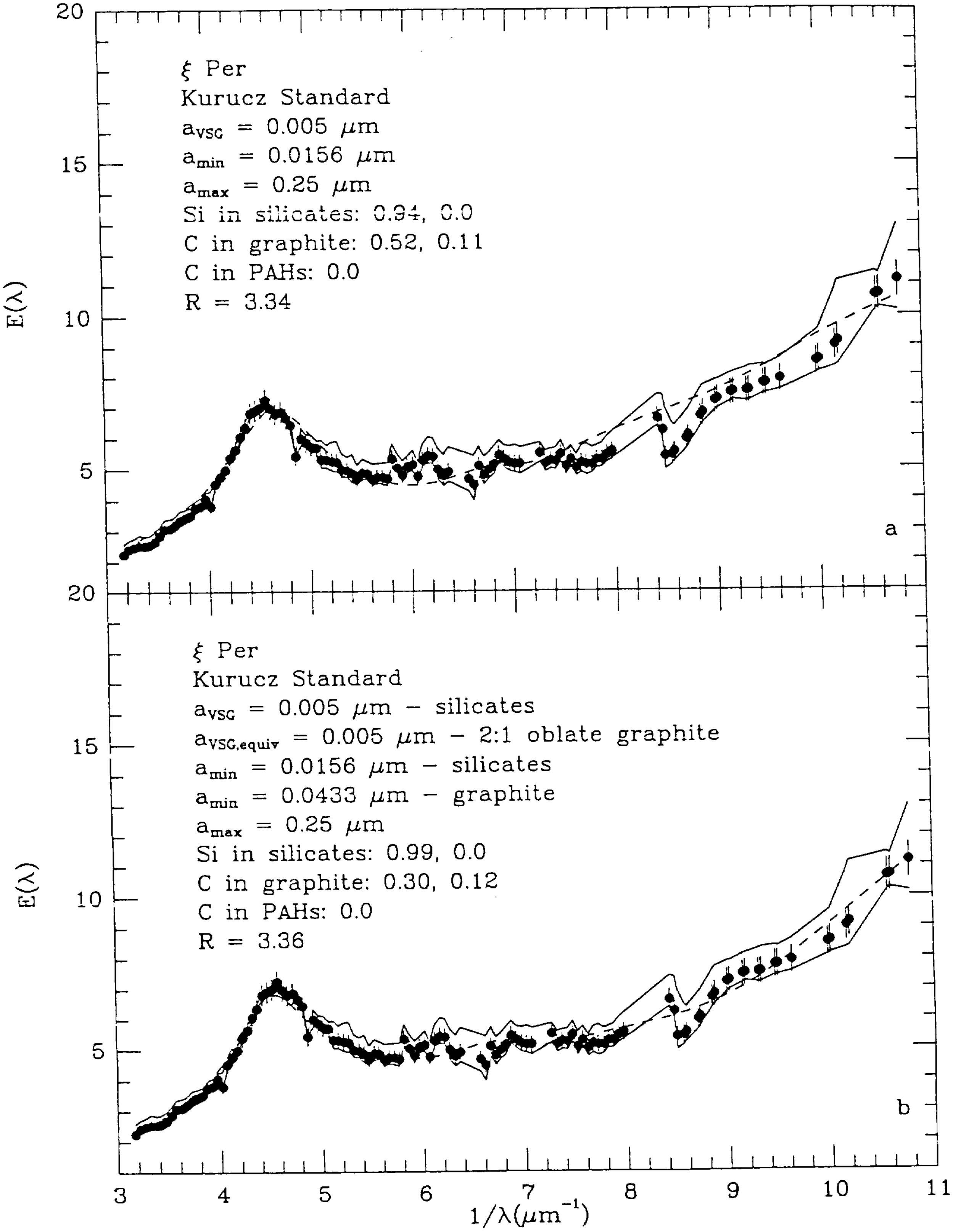ξ Per
Kurucz Standard
a_{VSG} = 0.005 μm
a_{min} = 0.0156 μm
a_{max} = 0.25 μm
Si in silicates: 0.94, 0.0
C in graphite: 0.52, 0.11
C in PAHs: 0.0
R = 3.34
a
ξ Per
Kurucz Standard
a_{VSG} = 0.005 μm – silicates
$a_{VSG,equiv}$ = 0.005 μm – 2:1 oblate graphite
a_{min} = 0.0156 μm – silicates
a_{min} = 0.0433 μm – graphite
a_{max} = 0.25 μm
Si in silicates: 0.99, 0.0
C in graphite: 0.30, 0.12
C in PAHs: 0.0
R = 3.36
b
E(λ)
20
15
10
5
1/λ(μm⁻¹)
3
4
5
6
7
8
9
10
11

Figure 6

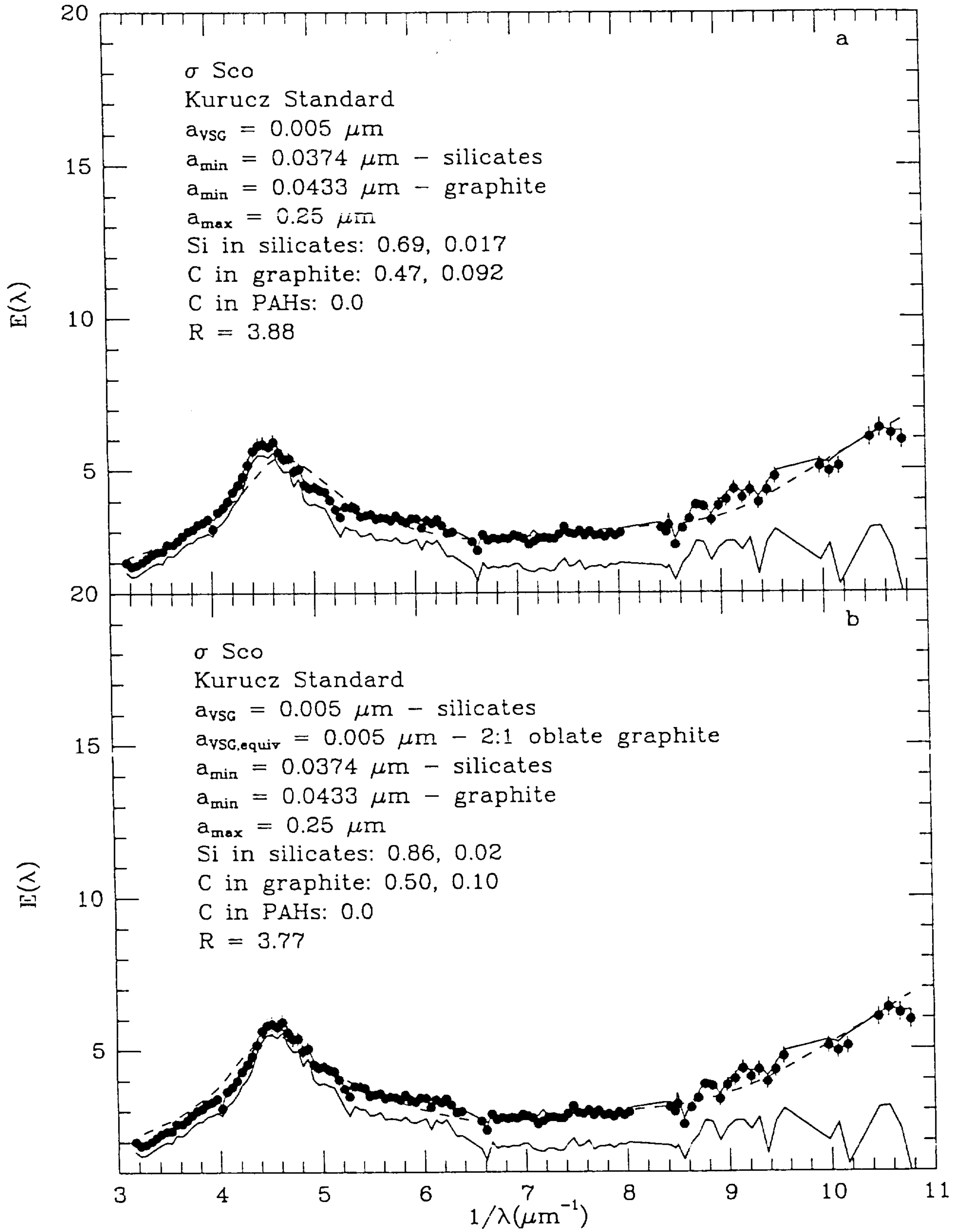
a
σ Sco
Kurucz Standard
a_{VSG} = 0.005 μm
a_{min} = 0.0374 μm – silicates
a_{min} = 0.0433 μm – graphite
a_{max} = 0.25 μm
Si in silicates: 0.69, 0.017
C in graphite: 0.47, 0.092
C in PAHs: 0.0
R = 3.88
b
σ Sco
Kurucz Standard
a_{VSG} = 0.005 μm – silicates
$a_{VSG,equiv}$ = 0.005 μm – 2:1 oblate graphite
a_{min} = 0.0374 μm – silicates
a_{min} = 0.0433 μm – graphite
a_{max} = 0.25 μm
Si in silicates: 0.86, 0.02
C in graphite: 0.50, 0.10
C in PAHs: 0.0
R = 3.77
E(λ)
20
15
10
5
3
4
5
6
7
8
9
10
11
1/λ(μm⁻¹)

Figure 7

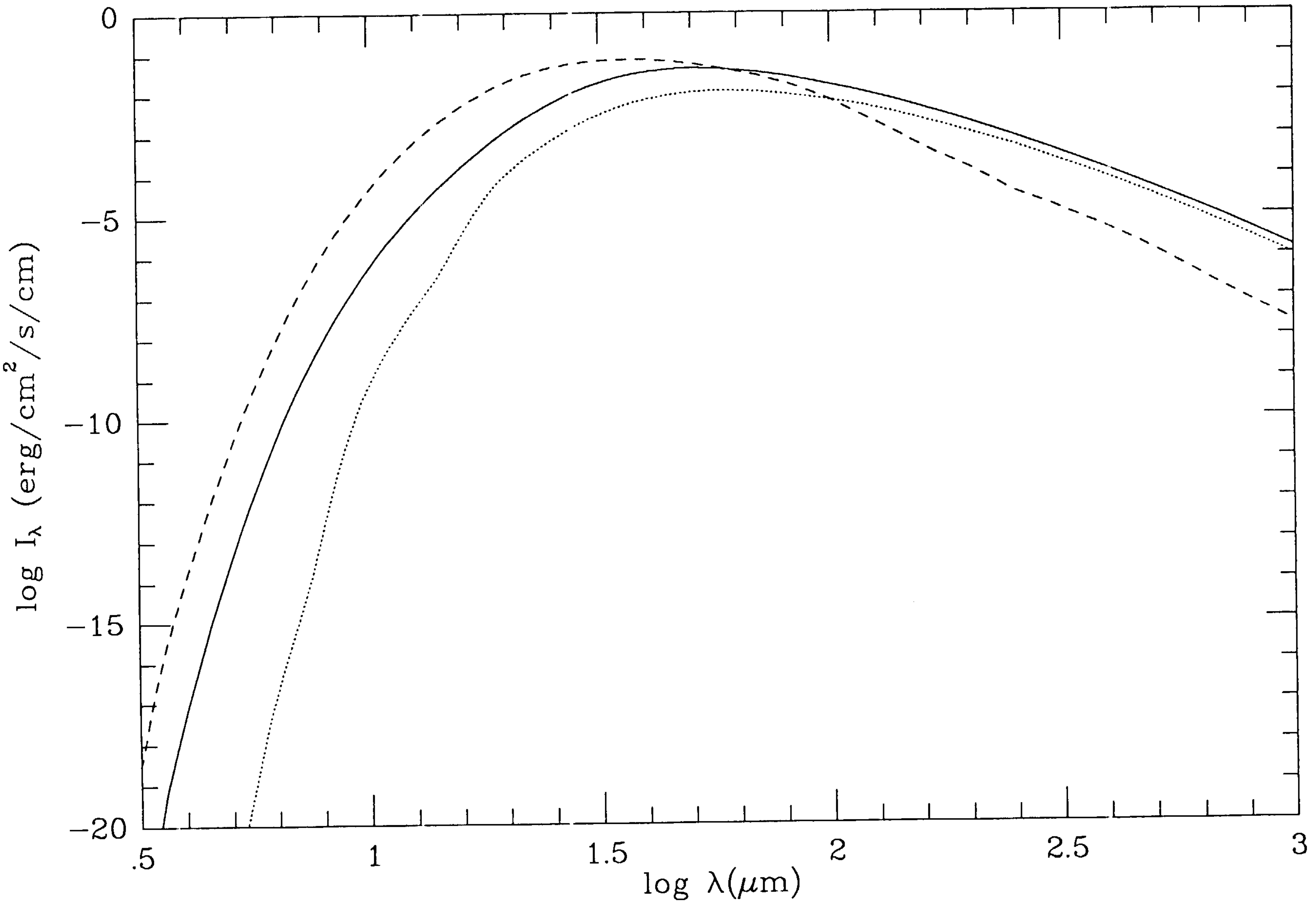

Figure 8

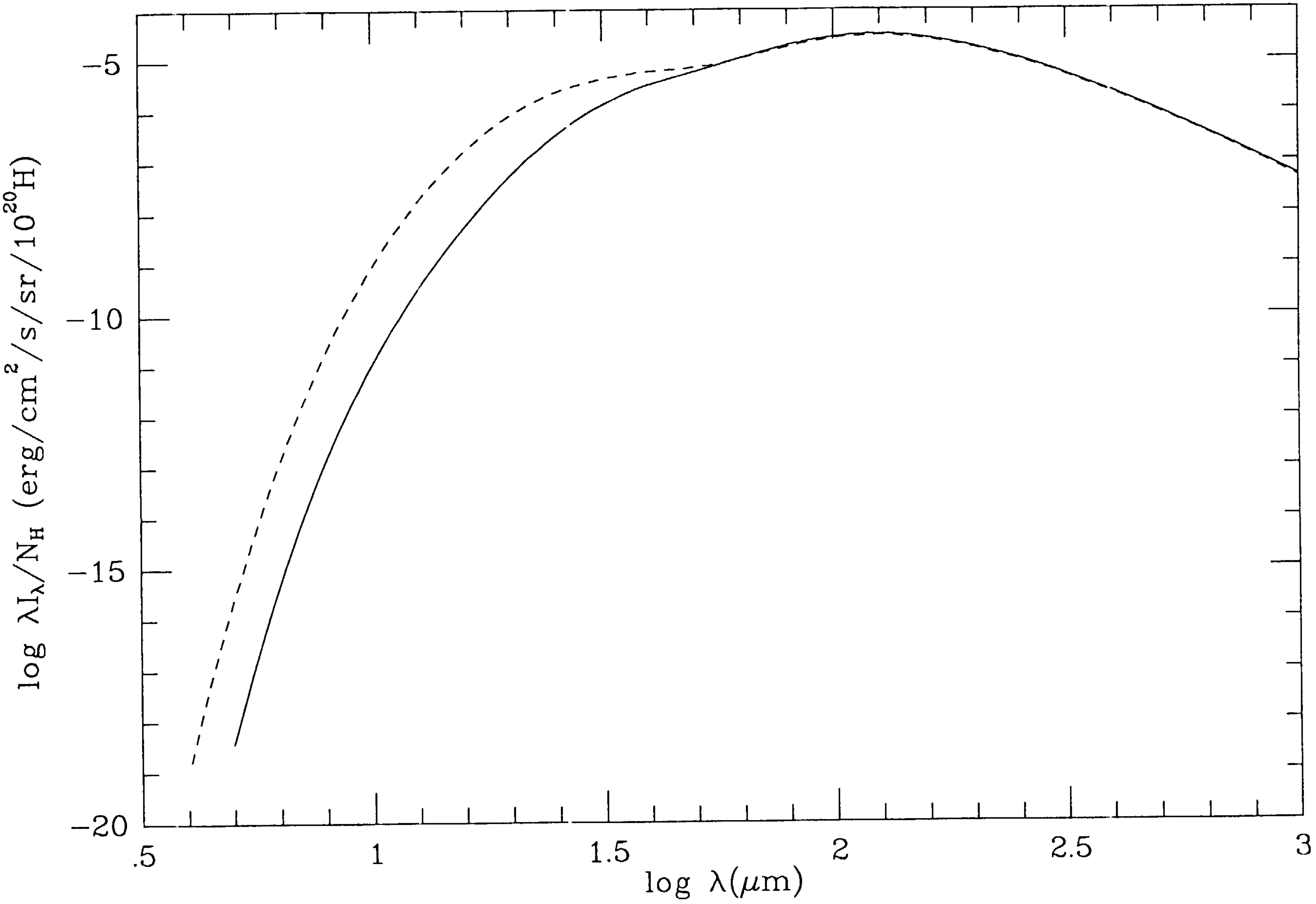

log $\lambda I_\lambda/N_H$ (erg/cm^2/s/sr/10^{20}H)
−5
−10
−15
−20
.5
1
1.5
2
2.5
3
log $\lambda(\mu m)$

Figure 9